ROYAL SOCIETY
OF CHEMISTRY

PAPER

Repulsion–dispersion parameters for the modelling of organic molecular crystals containing N, O, S and Cl†

Christina A. Gatsiou, Claire S. Adjiman ⓘD
and Constantinos C. Pantelides*

In lattice energy models that combine *ab initio* and empirical components, it is important to ensure consistency between these components so that meaningful quantitative results are obtained. A method for deriving parameters of atom–atom repulsion dispersion potentials for crystals, tailored to different *ab initio* models, is presented. It is based on minimization of the sum of squared deviations between experimental and calculated structures and energies. The solution algorithm is designed to avoid convergence to local minima in the parameter space by combining a deterministic low-discrepancy sequence for the generation of multiple initial parameter guesses with an efficient local minimization algorithm. The proposed approach is applied to derive transferable exp-6 potential parameters suitable for use in conjunction with a distributed multipole electrostatics model derived from isolated molecule charge densities calculated at the M06/6-31G(d,p) level of theory. Data for hydrocarbons, azahydrocarbons, oxohydrocarbons, organosulphur compounds and chlorohydrocarbons are used for the estimation. A good fit is achieved for the new set of parameters with a mean absolute error in sublimation enthalpies of 4.1 kJ mol^{-1} and an average rmsd$_{15}$ of 0.31 Å. The parameters are found to perform well on a separate cross-validation set of 39 compounds.

1 Introduction

Crystal Structure Prediction (CSP) has become a valuable tool for determining and understanding the solid states of an increasingly wide range of compounds and mixtures. As highlighted in the most recent (2016) blind test,[1] CSP methods for organic molecules are now applicable to a wide range of real systems, including salts, hydrates and large flexible molecules, with at least one successful prediction being achieved for each target system in the test.

Molecular Systems Engineering Group, Centre for Process Systems Engineering, Department of Chemical Engineering, Imperial College London, London SW7 2AZ, UK. E-mail: c.pantelides@imperial.ac.uk

Notwithstanding this significant progress, the results of the blind test also demonstrated some outstanding challenges for CSP methods specifically relating to energy ranking. In some cases, experimentally-observed structures for a given organic compound were deemed to have too high a lattice energy to occur in nature, and were consequently discarded from further consideration. Even methods that are generally successful in identifying the experimentally-observed crystal structures often fail to predict the experimentally-observed relative stability order.[2] While this may partly be due to the neglect of entropic contributions, the problem primarily arises from the insufficient accuracy of the lattice energy model in evaluating the energy differences between predicted structures, which can be as low as 1 kJ mol^{-1}.[3]

A variety of models have been developed and used in CSP for the calculation of the lattice energy, ranging from empirical force fields to electronic structure methods. Dispersion-corrected Density Functional Theory (DFT) models[4–6] have emerged as accurate methods for calculating energies,[1] with benchmark studies suggesting an uncertainty of 3 kJ mol^{-1} for absolute lattice energies.[7,8] However, the computational cost of these models precludes their use for the minimization of large numbers (tens or hundreds of thousands) of structures, a critical step in current CSP methodologies. On the other hand generic force fields such as COMPASS,[9] CVFF[10] and others are computationally efficient but of limited accuracy.[11,12] In view of these factors, the development of force fields that bridge the gap between these extremes has been an important step for all successful CSP methods. In this context, the models used in the sixth blind test included tailor-made potentials fitted to periodic *ab initio* data,[13] potentials derived from symmetry-adapted perturbation theory based on DFT (SAPT(DFT)) calculations,[14] and hybrid models combining isolated-molecule electronic structure calculations with empirical repulsion–dispersion potentials.[15–17] Further details of the different lattice energy models that have been used in CSP through the years and their performance can be found in the blind test papers[18–22] and review papers.[11,23]

In the CSP approach developed in our group,[24] different energy models are used for the global search step in which thousands of possible structures are generated (*CrystalPredictor*[16,17,25,26]) and in the refinement step in which the ranking of structures is finalized (*CrystalOptimizer*[27,28]). Recent developments in the model for the global search[16,17] have led to significant improvements in the accuracy of the force fields for large flexible molecules (such as molecule XXVI in the sixth blind test); in general, all experimentally-relevant structures are typically identified within 20 kJ mol^{-1} of the global minimum and carried through to the refinement stage.[16,17] The latter requires a higher degree of accuracy in the lattice energy. The intramolecular energy is calculated using local approximate models derived from the isolated-molecule *ab initio* energy[27] computed at a chosen level of theory. The intermolecular energy is derived by combining electrostatic interactions represented by distributed multipoles[15,29,30] derived from the isolated molecule charge density calculated at the same level of theory, and repulsion–dispersion interactions modelled by an empirical exp-6 potential with parameters taken from the literature such as the FIT potential,[31–37] W01 (ref. 38) or other parameterizations.[39]

The values of the repulsion–dispersion potential parameters used in most current methodologies were originally estimated from experimental crystal data analysed using an atomic charge representation of electrostatics, with charges

fitted to the HF/6-31G(d,p) charge density; intramolecular energy contributions were neglected.[10,18,39–41] As a result, such parameters are not necessarily consistent with more sophisticated electrostatic models such as those based on multipoles. In addition, only parameters relating to the most common atoms (C, N, O, H, Cl, F) were derived from extensive datasets. For atoms such as sulphur or bromine, parameters from a variety of literature sources are currently being used, a practice that is likely to result in inaccuracies. Furthermore, even within the set of atoms considered in the FIT and W01 parameterizations, some cross interactions (*e.g.*, O–N) were not fitted to experimental data; instead, they were approximated using geometric combining rules that are known to be of limited validity and may lead to inaccurate predictions.[42]

Overall, as has been stated elsewhere,[13] force fields should be carefully parameterized so that the different terms complement each other. In practical terms, repulsion–dispersion potentials need to be reparameterized for the specific electrostatics and intramolecular energy models with which they are intended to be used. There has been a recent effort[42] in this direction through the partial reparameterization of the FIT set using the B3LYP/6-31G** and B3LYP/6-311G** levels of theory and multipole expansions for the electrostatics. Focusing on O and N parameters, the work led to encouraging results, with experimental unit cells being reproduced to within 3% and hydrogen bond geometries and sublimation enthalpies between 7.4 and 9.0%.

In this paper, we present a systematic approach for the reparameterization of the repulsion–dispersion term using experimental structural and sublimation enthalpy data. The proposed algorithm can easily be used to derive empirical parameters consistent with different electrostatic models or levels of theory. Here, its applicability is demonstrated by deriving a set of exp-6 repulsion–dispersion potential parameters for C, H, N, O, S and Cl consistent with electrostatic interactions described by distributed multipoles derived from the M06/6-31G(d,p) level of theory. For the first time, this leads to parameters for sulphur that are consistent with the remaining parameter set and this is shown to lead to a significant improvement in performance.

2   The lattice energy model

To relate computational models of crystal structures to experimental data, it is generally assumed that the experimentally-observed crystals correspond to local minima of the Gibbs free energy. Moreover, given the relatively small contribution of entropic effects at low temperatures and the complexity associated with their calculation, the lattice energy is usually employed as an approximation of the free energy. Thus, the objective of CSP is the identification of all low-energy local minima in the lattice energy surface.

2.1   Defining the crystal structure

In frequently-used codes in CSP, such as the *CrystalOptimizer*[27,28] code on which we focus, the lattice energy of a crystal is a function of the following independent variables:

• The unit cell lengths and angles, collectively denoted by X.

• The positions of the centres of mass and the orientation of chemical entities within the unit cell, collectively denoted by β.

• The molecular conformational degrees of freedom (CDFs), *i.e.* bond lengths, angles and torsions, collectively denoted by θ.

It is also useful to introduce two dependent quantities, *i.e.* variables that are functions of the independent variables:

• $Q(\theta)$ denotes the set of parameters in the distributed multipoles[43] describing the molecule's electrostatic field for a given molecular conformation θ.

• $Y(\theta,\beta)$ denotes the Cartesian coordinates of all atoms in the unit cell, which depend on the molecular positions and orientations β and the molecular conformations θ.

2.2 Lattice energy model for CSP

The lattice energy of a crystal U_{latt} can be expressed as the sum of intramolecular and intermolecular energy contributions:

$$U_{\text{latt}}(X,\beta,\theta) = \Delta U^{\text{intra}}(\theta) + U^{e}(Y,X,Q) + U^{\text{rd}}(Y,X) \qquad (1)$$

where ΔU^{intra} is the intramolecular energy contribution (*i.e.*, the electronic energy after subtraction of the gas-phase internal energies of the chemical species in the crystal weighted by their stoichiometric coefficients) and U^{e} and U^{rd} represent, respectively, the intermolecular electrostatic and repulsion–dispersion contributions.

The intramolecular contribution $\Delta U^{\text{intra}}(\theta)$ in the above expression is typically computed *via* a QM evaluation of the conformational energy at given θ.

The intermolecular electrostatic model is based on a distributed multipole representation of electrostatics, placing an expansion up to the hexadecapole moment at each atomic position (as in *DMACRYS*[15] and hence *CrystalOptimizer*[27]). The GDMA program[30] is used to derive the parameters $Q(\theta)$ from the isolated molecule wavefunction;[29] the latter is also determined by the QM calculation used for the computation of $\Delta U^{\text{intra}}(\theta)$ at given θ. The intermolecular electrostatic energy, U^{e}, is calculated as the sum of interactions between multipoles on atomic sites of different molecules. Such a representation of electrostatics has been shown to be successful in predicting highly-directional (anisotropic) lone-pair interactions, π–π stacking in aromatic rings and hydrogen bond geometries in organic crystals.[44–46]

The repulsion–dispersion component of the intermolecular energy, U^{rd}, is calculated as the sum of all repulsion–dispersion interactions within a predefined cutoff. Each interaction, U^{rd}_{ij}, between two atoms of types i and j occurring in two different molecules and separated by a distance r is described through an isotropic atom–atom Buckingham potential:

$$U^{\text{rd}}_{ij}(r) = A_{ij} \exp\left(-r/B_{ij}\right) - \frac{C_{ij}}{r^{6}} \qquad (2)$$

where the interatomic separation r between any two atoms can be derived from X and Y. In many current CSP methodologies, the values of the adjustable parameters A_{ij}, B_{ij}, C_{ij} for atoms of the same type ($i = j$) are usually taken from the FIT set;[18,31–36] for unlike atom types ($i \neq j$), the parameters are usually computed *via* combining rules:

$$A_{ij} = \sqrt{A_{ii}A_{jj}}; \quad B_{ij} = \frac{B_{ii} + B_{jj}}{2}; \quad C_{ij} = \sqrt{C_{ii}C_{jj}}, \qquad (3)$$

although more recently,[42] parameters A_{ij} and C_{ij} for some atom types have been regressed directly from data. The most common elements C, N, O, S, F, Cl are treated as transferable atom types in the FIT parameterization, but three distinct atom types are employed for hydrogen, namely hydrogen bonded to carbon, H_C; hydrogen bonded to nitrogen, H_N; and hydrogen bonded to oxygen, H_O.

Finally, in calculating U^e and U^{rd}, summations of intermolecular atom–atom interactions between the central unit cell and other cells in the crystal must be computed. This is done *via* a combination of direct and Ewald summations within a predefined cutoff which is set to 15 Å by default.[15]

2.3 Lattice energy model for parameterization

While the intramolecular energy plays an important role in CSP for flexible molecules, accounting for conformational changes leads to significant increases in the computational cost of energy evaluations. As a result, in keeping with previous work on the parameterization of force fields for CSP,[31–36] we rely on a dataset that contains structures of relatively rigid molecules with no flexible torsions. For such a dataset, intermolecular interactions within the solid will not significantly distort the conformation of the molecule, and the experimental values of the molecular conformation variables, θ^{exp}, can be expected to be close to those for the global minimum in the QM energy function for the isolated molecule, θ^{gas}. However, due to experimental error and theoretical approximations, there are typically some small differences between θ^{exp} and θ^{gas}. Thus, for the purpose of the calculations, we fix the CDFs to the values of θ^{gas} consistent with the chosen level of the theory. The intramolecular energy, ΔU^{intra}, is then equal to zero and as a result the lattice energy model takes the simplified form:

$$U_{latt}(X, \beta; \theta^{gas}) = U^e(Y, X, Q(\theta^{gas})) + U^{rd}(Y, X, p) \tag{4}$$

where p denotes the set of model parameters A_{ij}, B_{ij}, C_{ij} for all atom–atom interactions.

To assess the validity of the lattice energy model, and in particular of the parameter values p, we seek a local energy minimum close to the given experimental structure, (X^{exp}, β^{exp}). The lattice energy computed for a given p, denoted by $U_{latt}^*(p)$, is given by:

$$U_{latt}^*(p) = \min_{X, \beta} U^{latt}(X, \beta; p, \theta^{gas} | X^{exp}, \beta^{exp}) \tag{5}$$

where the notation "X^{exp}, β^{exp}" denotes that the values X^{exp}, β^{exp} are used as the starting point for the local minimization of the lattice energy; the semicolon preceding p and θ^{gas} indicates that these quantities remain fixed throughout the lattice energy minimization. The above minimization problem is solved subject to all appropriate symmetry considerations, and its solution determines the geometry of the predicted structure, denoted by (X^*, β^*).

The quantities U_{latt}^* and (X^*, β^*) form the basis for comparison between predicted and experimental structures, as discussed in the next section.

3 Parameter estimation

An extensive set of experimental crystal property data is required to determine appropriate values for the repulsion–dispersion parameters. More specifically, the

properties that can be most directly related to the lattice energy model are the geometries of experimentally-observed crystal structures determined by diffraction methods, and sublimation enthalpies.

3.1 Quantifying deviations in crystal geometry

The structural features predicted by the model can be assessed by comparison to different types of experimental structure data as available in the Cambridge Structural Database (CSD).[47] As experimental X-ray diffraction (XRD) data are subject to relatively small uncertainties, they are valuable for parameter estimation. However, there are well-known difficulties in determining hydrogen positions[39] and in determining the bond lengths of polar or high-order bonds (such as $C\equiv N$, $C=C$, $C\equiv C$) due to the fact that interatomic nuclei distances in XRD are defined as distances between electron densities.[48,49] Thermal effects may be another source of error in structural data: typically, unit cell lengths in organic crystals may increase by around 3% over a temperature range of several hundred degrees.[50]

In order to minimize the potential effects of experimental errors, our study applied the following criteria in selecting appropriate experimental crystallographic data from the CSD:

1. Relatively rigid molecules should be chosen.

2. Solvate and hydrate crystals are avoided.

3. Structures at high pressures (above ambient pressure) and above room temperature are rejected.

4. Single-crystal diffraction data are preferable over powder diffraction data.

5. Structures resolved *via* neutron scattering are preferred when available.

6. Structures resolved with XRD with an X-ray discrepancy factor (R) exceeding 5% are normally rejected, unless their sublimation enthalpies are also available or other criteria are met.

Several distance metrics are available for quantifying the deviation between two given crystal structures.[51] In our work, the deviation between experimental and predicted structures for a crystal i is described by a metric $G_i(p)$ that consists of two contributions. The first contribution measures the relative deviations between the experimental and predicted unit cell parameter vectors, X_i^{exp} and X_i^* respectively:

$$\frac{1}{N_{X_i}} \sum_{j=1}^{N_{X_i}} \left(\frac{X_{ij}^{exp} - X_{ij}^*(p)}{X_{ij}^{exp}} \right)^2 \qquad (6)$$

where N_{X_i} is the number of unit cell parameters not constrained by symmetry, and the jth such parameter in crystal i is indicated by subscript j. The second contribution measures the deviations between atomic positions within the asymmetric unit. Given the fractional coordinates $Y'_{x,i,j}$, $Y'_{y,i,j}$ and $Y'_{z,i,j}$‡ of an atom j in the asymmetric unit of a crystal i, its relative position vector with respect to a reference atom,§ denoted by the subscript "ref", is given by:

$$\delta Y'_{x,i,j} = Y'_{x,i,j} - Y'_{x,i,\text{ref}}; \quad \delta Y'_{y,i,j} = Y'_{y,i,j} - Y'_{y,i,\text{ref}}; \quad \delta Y'_{z,i,j} = Y'_{z,i,j} - Y'_{z,i,\text{ref}} \qquad (7)$$

---

‡ Fractional coordinates can be computed directly from the Cartesian coordinates Y and the unit cell parameters X, *i.e.* $Y' = Y'(X,Y)$.

§ The first heavy atom listed in the SHELX file.

The contribution of atomic positions to the deviation measure $G_i(p)$ between experimental and predicted structures for crystal i is then given by:

$$\frac{1}{3(N_{\text{asym}_i} - 1)} \sum_{j=1}^{N_{\text{asym}_i}-1} \left(\delta Y_{x,i,j}^{\prime\text{exp}} - \delta Y_{x,i,j}^{\prime*}(p)\right)^2 + \left(\delta Y_{y,i,j}^{\prime\text{exp}} - \delta Y_{y,i,j}^{\prime*}(p)\right)^2$$

$$+ \left(\delta Y_{z,i,j}^{\prime\text{exp}} - \delta Y_{z,i,j}^{\prime*}(p)\right)^2 \tag{8}$$

where N_{asym_i} is the number of atoms in the asymmetric unit cell for crystal i.

The calculation of the relative position vectors is described in detail in the ESI.† In order to avoid introducing an inherent offset in the deviation metric $G_i(p)$, the fractional atomic coordinates in the experimental crystal are computed based on the predicted (rather than the experimental) molecular conformation. This is appropriate provided that the differences between θ^{gas} and θ^{exp} are small, a condition that needs to be verified when constructing the experimental dataset.

Overall, the function $G_i(p)$ used as a measure of similarity between experimental and predicted structures is defined as:

$$G_i(p) = \frac{1}{N_{X_i}} \sum_{j=1}^{N_{X_i}} \left(\frac{X_{ij}^{\text{exp}} - X_{ij}^*(p)}{X_{ij}^{\text{exp}}}\right)^2 + \frac{1}{3(N_{\text{asym}_i} - 1)}$$

$$\times \sum_{j=1}^{N_{\text{asym}_i}-1} \left(\delta Y_{x,i,j}^{\prime\text{exp}} - \delta Y_{x,i,j}^{\prime*}(p)\right)^2 + \left(\delta Y_{y,i,j}^{\prime\text{exp}} - \delta Y_{y,i,j}^{\prime*}(p)\right)^2$$

$$+ \left(\delta Y_{z,i,j}^{\prime\text{exp}} - \delta Y_{z,i,j}^{\prime*}(p)\right)^2 \tag{9}$$

It is worth noting that the above expression aims to balance the contributions of various terms *via* the application of appropriate scaling factors. Thus, relative (rather than absolute) deviations are used for the unit cell parameters. No such scaling is needed for the position vectors as they are already normalized. Moreover, since the two summations may comprise very different numbers of terms, the first one is divided by the number of unit cell parameters not constrained by symmetry, N_{X_i}, and the second one by the number of fractional coordinates describing the asymmetric unit, $3(N_{\text{asymi}}-1)$.

The quantity $G_i(p)$ is directly incorporated in the objective function of the parameter estimation problem. In analysing the quality of the results of the parameter estimation, the root mean squared deviation of the 15 molecule coordination sphere, rmsd_{15},[52] is used as an additional measure of similarity between predicted and experimental crystals.

3.2 Quantifying deviations in sublimation enthalpy

The accuracy of the computed lattice energies can be assessed from sublimation enthalpies reported in thermophysical properties databases such as NIST[53] and DETHERM.[54] Uncertainties in measured sublimation enthalpies can be very large due to several factors such as polymorphism, a lack of standards for compounds with low vapour pressures, chirality, systematic errors associated with the measurement techniques and further errors that can be introduced in measurements by adjustment to a reference temperature (which is necessary when comparing different measurements).[55] Based on 451 measurements of 80

compounds, Chickos et al.[55] estimated the average uncertainty of sublimation enthalpies to be 4.9 kJ mol^{-1}. Consequently, our study does not make use of any sublimation enthalpy measurement with a reported error exceeding 4.9 kJ mol^{-1}.

A calculated enthalpy of sublimation at temperature T and pressure P, $\Delta H^*_{\text{sub}}(T,P)$, can be obtained from the predicted lattice energy U^*_{latt} by the following commonly-used approximation:[56–58]

$$\Delta H^*_{\text{sub}}(T,P) \approx -U^*_{\text{latt}}(T=0 \text{ K}, P)) - 2RT, \qquad (10)$$

in which the zero-point energy is neglected. A derivation of eqn (10) is given in the ESI.†

In previous studies by Arnautova et al.[59] and Gavezzotti,[60] computed lattice energies were directly compared to experimental sublimation enthalpies without any correction, an approach justified by the authors on the basis of uncertainty in the sublimation enthalpy data. We prefer to apply the correction shown in eqn (10) in order to reduce any systematic error in the comparison between predicted and experimental values. Thus, we employ the following deviation function as a measure of the difference between the experimental and predicted sublimation enthalpies for a given crystal i:

$$E_i(p) = \left(\frac{\Delta H^{\text{exp}}_{\text{sub},i} - \Delta H^*_{\text{sub},i}(p)}{\Delta H^{\text{exp}}_{\text{sub},i}} \right)^2 \qquad (11)$$

3.3 Obtaining globally optimal parameter estimates

Parameter estimation aims to determine the values of parameters p for which the calculated quantities best match the experimentally-observed quantities. This can be expressed mathematically as the minimization of a combined deviation metric $R(p)$:

$$\min_p R(p) \equiv \sum_{i \in I_G} w^G_i G_i(p) + \sum_{i \in I_E} w^E_i E_i(p) \qquad (12)$$

where I_G and I_E are the sets of crystal structures for which we have reliable experimental data on the geometry and sublimation enthalpy respectively. In general, I_E is a subset of I_G, reflecting the fact that reliable sublimation enthalpy measurements may not be available for all crystal structures under consideration. The constants w^G_i and w^E_i are non-negative weights that can be adjusted to reflect differences in the reliability between different experimental data and to yield a desirable trade-off between geometry and energy reproduction.

In general, we seek to establish the values of p that lie within given lower and upper bounds, p^l and p^u respectively, and lead to a globally minimal value of $R(p)$. To compute $R(p)$ at a given set of parameter values p, we need to perform the lattice energy minimization (5) for each crystal structure $i \in I_G$ starting from the corresponding experimental structure. Once the optimal solution is obtained, we can compute the geometry deviation $G_i(p)$ and, if $i \in I_E$, the sublimation enthalpy deviation $E_i(p)$. The quantities $G_i(p)$ and $E_i(p)$ can then be used to compute $R(p)$ via eqn (12). Overall, this is a relatively expensive computation as it involves a large number of crystal structure minimizations, but these can be carried out in parallel.

A more serious challenge for the reliable solution of problem (12) is that the objective function $R(p)$ may have multiple local minima, in which case the solution obtained via the application of standard local minimization algorithms may

depend on the starting points (*i.e.* the initial guesses) for the parameters p. In order to increase the likelihood of identifying the globally optimal parameter vector, we adopt a step-wise approach involving the generation of many starting points in the space of parameters p, followed by a gradient-based local minimization from selected starting points:

1. Compute the reference quantity $R(p^{\text{FIT}})$ where p^{FIT} are the values of the parameters in the existing FIT parameterization.

2. Generate N points p^k, $k = 1, \ldots, N$, in the parameter space by means of a Sobol' sequence[61,62] within the defined bounds $[p^l, p^u]$. The advantages of low-discrepancy (such as Sobol') sequences over other methods (*e.g.* Monte Carlo sampling or uniform grids) for efficiently searching multivariable domains are well established.[63]

3. For each point p^k, evaluate the corresponding $R(p^k)$ as described above; discard all points for which $R(p^k)$ exceeds the reference value $R(p^{\text{FIT}})$ by more than a specified factor α (*e.g.* 5) as these are unlikely to yield parameter estimates that are better than the FIT one.

4. Starting from p^k as the initial guess, perform the local minimization (eqn (12)) to obtain a (locally) optimal parameter estimate $p^{*,k}$ with a corresponding objective function value $R(p^{*,k})$. As described in the ESI,† a sequential quadratic programming (SQP) algorithm with a Broyden–Fletcher–Goldfarb–Shanno (BFGS)[64] update of the Hessian matrix is used for this purpose.

5. Choose the solution $p^{*,k}$ with the lowest corresponding value $R(p^{*,k})$ as the best parameter estimate p^*.

A flowchart of the overall parameter estimation methodology is shown in Fig. 1.

3.4 Cross-validation of optimal parameter estimates

To further assess the quality of the optimal parameter estimates p^* obtained by the procedure described in the previous section, we examine its ability to reproduce experimental geometry and sublimation enthalpy data both for the structures used for the estimation, and for a separate set of structures reserved for cross-validation purposes.

The quality of geometry reproduction is assessed based on the usual $\text{rmsd}_{15,i}$ measure between an experimental and predicted crystal i calculated using the *COMPACK*[52] code. We also consider the rmsd_{15} averaged over a set of crystal structures.

For assessing the quality of sublimation enthalpy prediction for each individual crystal i, we use the Absolute Deviation (AD_i) defined as:

$$\text{AD}_i = \left| \Delta H^{\text{exp}}_{\text{sub},i} - \Delta H^*_{\text{sub},i} \right| \tag{13}$$

as well as the average and maximum values of AD over a set of N_{str} crystal structures:

$$\text{AAD} = \frac{1}{N_{\text{str}}} \sum_{i=1}^{N_{\text{str}}} \left| \Delta H^{\text{exp}}_{\text{sub},i} - \Delta H^*_{\text{sub},i} \right| \tag{14}$$

and

$$\text{maxAD} = \max_{i=1,\ldots,N_{\text{str}}} \left| \Delta H^{\text{exp}}_{\text{sub},i} - \Delta H^*_{\text{sub},i} \right| \tag{15}$$
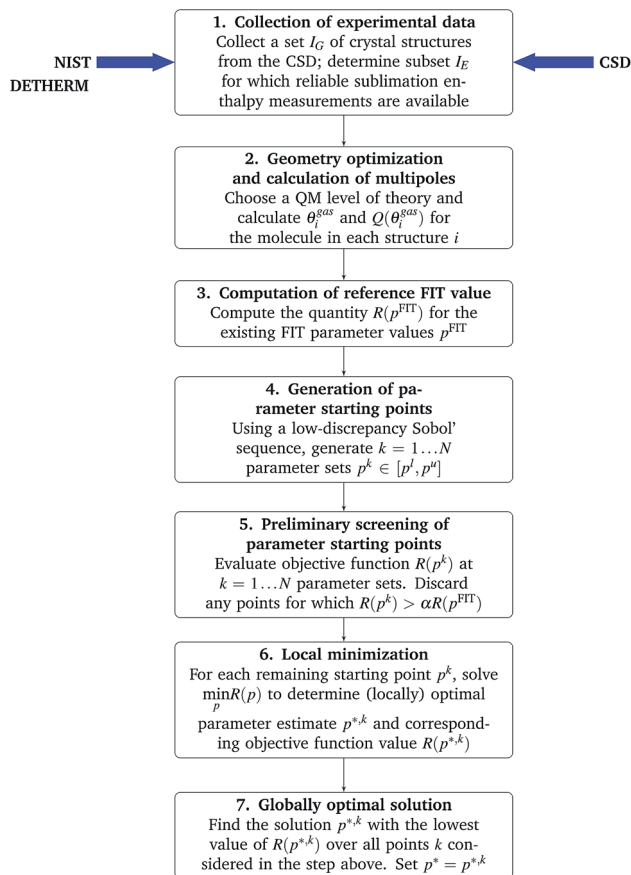
1. Collection of experimental data
Collect a set I_G of crystal structures from the CSD; determine subset I_E for which reliable sublimation enthalpy measurements are available

NIST
DETHERM

CSD

2. Geometry optimization and calculation of multipoles
Choose a QM level of theory and calculate θ_i^{gas} and $Q(\theta_i^{gas})$ for the molecule in each structure i

3. Computation of reference FIT value
Compute the quantity $R(p^{FIT})$ for the existing FIT parameter values p^{FIT}

4. Generation of parameter starting points
Using a low-discrepancy Sobol' sequence, generate $k = 1 \ldots N$ parameter sets $p^k \in [p^l, p^u]$

5. Preliminary screening of parameter starting points
Evaluate objective function $R(p^k)$ at $k = 1 \ldots N$ parameter sets. Discard any points for which $R(p^k) > \alpha R(p^{FIT})$

6. Local minimization
For each remaining starting point p^k, solve $\min_p R(p)$ to determine (locally) optimal parameter estimate $p^{*,k}$ and corresponding objective function value $R(p^{*,k})$

7. Globally optimal solution
Find the solution $p^{*,k}$ with the lowest value of $R(p^{*,k})$ over all points k considered in the step above. Set $p^* = p^{*,k}$

Fig. 1 Flowchart of the methodology for parameter estimation.

We generally aim to derive parameter estimates for which the average values AAD and rmsd$_{15}$ do not exceed 5 kJ mol^{-1} and 1 Å respectively.[22]

4 Parameterization strategy

For a parameter estimation study involving N_A distinct types of atoms, there are $N_A(N_A + 1)/2$ possible interaction pairs that need to be considered, and consequently $3N_A(N_A + 1)/2$ repulsion–dispersion parameters that need to be estimated from experimental data. Overall, even for relatively small N_A, this is a difficult and computationally expensive problem to solve.

An approach commonly used for reducing the parameter space is to use combining rules for the parameters describing interactions between atoms of different types. The use of such combining rules for the dispersion coefficient does have some physical justification at the level of the Unsöld approximation to the r_{ij}^{-6} dispersion. However, other rules are known to be limited in their accuracy,[65] and their use may lead to lower quality of predictions in crystal structure calculations.[32,42,66] Therefore, in this study we prefer not to use combining rules,

relying instead on the estimation of the cross-interaction parameters directly from experimental data.

On the other hand, and in common with the approach adopted by Pyzer-Knapp et al.,[42] we do hold the exponential B_{ij} parameters fixed at the FIT values: the shape of the potential is very sensitive to even small changes in these parameters, which renders their numerical handling as part of the parameter estimation procedure problematic.

Finally, in order to make the problem computationally manageable and ensure compatibility and transferability of the different sets of parameters, the parameter estimation is carried out in a sequential manner as shown schematically in Fig. 2. Similarly to the work of Sun,[67] optimal parameters for carbon and hydrogen (H_c) are determined first based on experimental data for hydrocarbons. These are then fixed for the subsequent steps, and interaction parameters for other atom pairs are estimated from data on appropriate compounds.

5 Illustration of methodology

The methodology proposed in this paper is illustrated for the estimation of parameters for the $C\cdots C$, $C\cdots H_C$ and $H_C\cdots H_C$ interactions using experimental data for hydrocarbon crystals (cf. the top box in Fig. 2). As indicated in the flow-chart in Fig. 1, we start by collecting relevant experimental data based on the general criteria described in Section 3.1. The experimental crystallographic data and energetic data collected for hydrocarbons are listed in Table S1 of the ESI.† This consists of 19 compounds and exhibits a diversity of hybridizations not present in the training sets for the FIT parameterization.

We then perform an isolated-molecule gas-phase QM calculation for each molecule using Gaussian09 (ref. 68) with the M06 (ref. 69) functional and a 6-31G(d,p) basis set. The resulting wavefunctions are used to generate multipole moments via the distributed multipole analysis method[43] as implemented in the GDMA 2.2 program.[43]

We now fix the three B_{ij} parameters to their FIT values, and aim to determine optimal estimates for the 6 A_{ij} and C_{ij} parameters; the latter constitute our parameter vector p. For the purposes of this estimation, we will allow p to vary within ±40% of the FIT values. As explained in Section 3.3, in order to increase
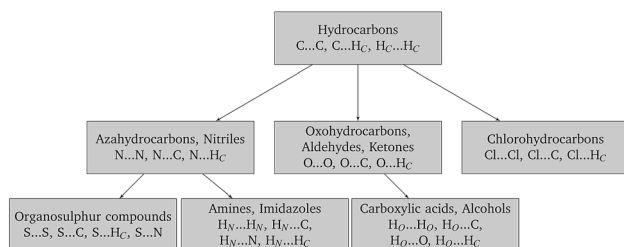
Fig. 2 Parameterization tree. Each box indicates the type of molecules for which experimental crystal structures are used for the estimation (first line) and the interaction parameters being estimated from these data (second line). The values of the parameters estimated in each box are thereafter held constant in the estimations corresponding to the boxes below, as indicated by the direction of the arrows.

the probability of obtaining globally optimal parameter estimates, we use a Sobol' sequence to generate 1000 starting points p^k, $k = 1, ..., 1000$.

Before proceeding with actually performing local minimizations of function $R(p)$ (cf. eqn (12)) starting from some of the above points, it is instructive to gain some insight as to the appropriate choices of the weighting factors w_i^G and w_i^E. For simplicity, we use the same weight values (w^G or w^E) for all 19 structures i. We consider 15 distinct combinations of these weights as shown in Table 1, and evaluate the objective function $R(p^k)$ for each such combination. The 19 000 local lattice energy minimizations required for evaluating $R(p^k)$, $k = 1, ..., 1000$ are performed with *DMACRYS* at 0 Pa pressure.

For each weight combination, having evaluated the objective function $R(p^k)$ at the 1000 Sobol' points p^k, we select the Sobol' point with the lowest value of the objective function. This serves as an approximation to the optimal parameter estimate $p*$ that might be obtained using that particular combination of weights. The solutions arising from different weight combinations are compared in Fig. 3 based on the geometry and sublimation deviation functions, $G(p*)$ and $E(p*)$, averaged over the 19 crystal structures under consideration.

The maximum and minimum values of $G_i(p*)$ across all 19 crystal structures i are also depicted on the horizontal axis of Fig. 3 while the maximum and minimum $E_i(p*)$ are shown against the vertical axis. We note that several weight ratios lead to the same solution; in fact, only 4 distinct solutions are obtained, as depicted by the solid symbols in Fig. 3. Based on these results, the weights $w^G = 1$ and $w^E = 1$ appear to offer both the best trade-off between geometry and energy errors, and the smallest variation of these errors across the different structures being considered. Accordingly, these values are chosen to be used throughout our parameter estimation methodology in this paper.

The values of $R(p^k)$ for the weights $w^G = w^E = 1$ at the 1000 points p^k are plotted in Fig. 4. The corresponding reference value $R(p^{FIT})$ for the FIT parameter values p^{FIT} is also shown. We note that the FIT parameter point, p^{FIT}, lies among the lowest points in this figure, which suggests that the FIT parameter values are

Table 1 Combinations of objective function weights considered

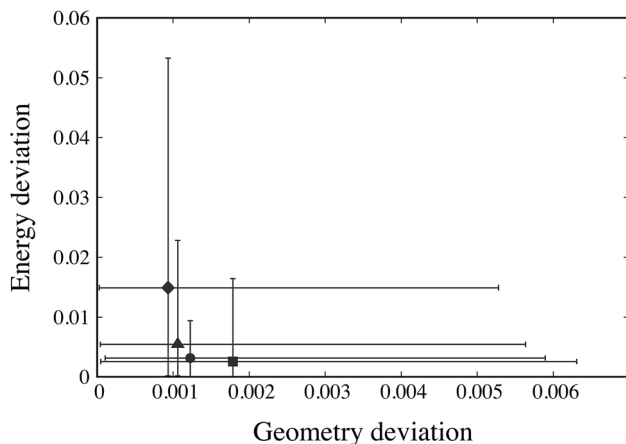| w^G	w^E
100	1
50	1
20	1
15	1
10	1
5	1
2	1
1	1
1	2
1	5
1	10
1	15
1	20
1	50
1	100

Fig. 3 Geometry and energy deviation functions, $G(p*)$ and $E(p*)$, at (approximately) optimal points $p*$ obtained using different weight ratios $w^G : w^E$. Solid points indicate $G_i(p*)$ and $E_i(p*)$ values averaged across all 19 structures i. There are 4 distinct such points: diamond (◆): weight ratio 100 : 1; triangle (▲): weight ratios 50 : 1, 20 : 1, 15 : 1; circle (●): weight ratios 10 : 1, 5 : 1, 2 : 1, 1 : 1; and square (■): weight ratios 1 : 2, 1 : 5, 1 : 10, 1 : 15, 1 : 20, 1 : 50, 1 : 100. The horizontal and vertical line segments through each point indicate the range of values of, respectively, $G_i(p)$ and $E_i(p)$ across all 19 structures.
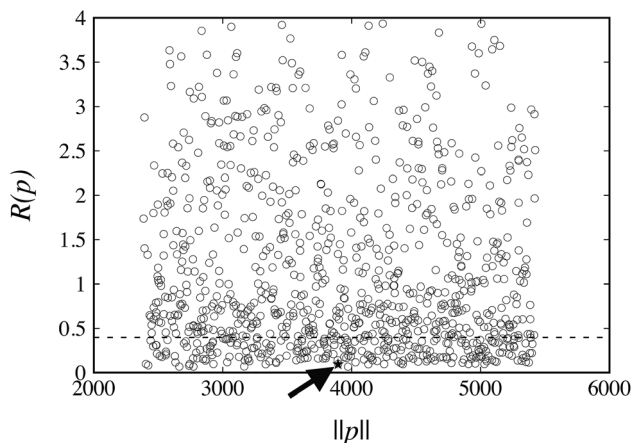
Fig. 4 Distribution of objective function values, $R(p^k)$, obtained with weights $w^G = w^E = 1$, at starting parameter points p^k, $k = 1, \ldots, 1000$ (denoted by open circles, ○). Symbol ★, highlighted with the arrow, indicates the corresponding objective function value $R(p^{FIT})$ evaluated at the FIT parameter values. The dashed line signifies the cutoff applied for the subsequent local minimization step.

already good estimates, a result that was expected given the similarity between the training set used in this work for hydrocarbons and that used by Williams *et al.*[31]

The FIT reference value $R(p^{FIT})$ allows us to prune out any Sobol' points that are unlikely to result in an improved fit of the experimental data over the already available FIT parameters (*cf.* step 5 of the algorithm in Fig. 1). Here we apply a cutoff ratio α of approximately 5, which excludes all but 250 of the original

Sobol' points from further consideration. We then solve the optimization problem expressed by eqn (12) starting from each of the remaining 250 points. The initial objective function values $R(p^k)$ and the final objective function values after local minimization, $R(p^{*,k})$, are shown in Fig. 5. It can be seen that the minimization does result in a significant reduction of the objective function $R(p)$. The results suggest a "flat" objective function with many broad and shallow minima; however, it is also possible that some of the points are not true local minima, but simply arise due to premature termination of the challenging local minimization.

The parameter values p^* resulting in the lowest objective function value are given in Table 2 where they are also compared with the original FIT parameters. A comparison of the corresponding objective function values is presented in Table 3. The objective function value for p^* is 63% lower than the corresponding value for the FIT parameters. The new parameters also achieve 23% and 72% reductions in the geometry and energy deviation functions respectively. Overall, the new parameters yield a significantly better reproduction of both the geometries and energies of the crystals in the training set even in the case of such
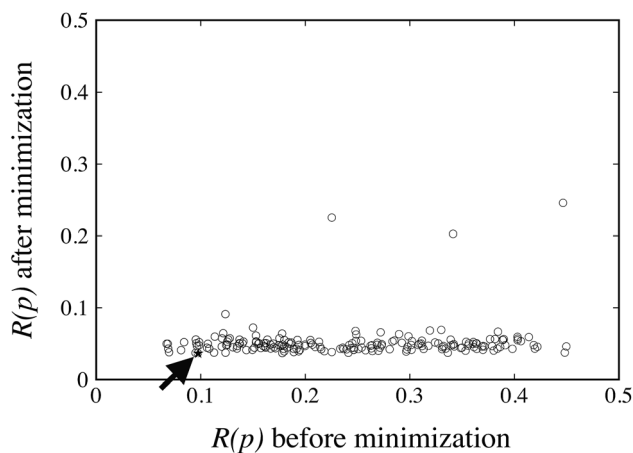
Fig. 5 Local minimization results for the 250 initial Sobol' points. Objective function value after minimization *vs.* objective function value before local minimization (denoted by open circles, ∘). The best solution is marked with a star (★).

Table 2 Exp-6 potential parameters for hydrocarbons obtained as a result of the refinement

Atom type		FIT[a]			This work		
i	j	A_{ij}/eV	B_{ij}/Å	C_{ij}/eV Å^6	A_{ij}/eV	B_{ij}/Å	C_{ij}/eV Å^6
C	C	3832.147	0.278	25.287	2299.288	0.278	18.020
C	H$_C$	689.537	0.272	5.979	449.3172	0.272	6.265
H$_C$	H$_C$	124.072	0.267	1.414	173.559	0.267	1.957

[a] Parameter values taken from the CPOSS website.[37]

Table 3 Comparison of objective function values between p^{FIT} and p^* for the hydrocarbon test set. The geometry and energy deviation functions averaged over the 19 structures under consideration are also compared

Parameter set	$R(p)$	$\frac{1}{N_{str}} \sum_{i=1}^{N_{str}} G_i(p)$	$\frac{1}{N_{str}} \sum_{i=1}^{N_{str}} E_i(p)$
FIT p^{FIT}	0.098	0.036	0.063
Best solution p^*	0.037	0.028	0.010

a relatively simple and well-studied parameter set. Further details of the quality of fit for each individual structure are presented in Table S4 of the ESI.†

6 Results and discussion

In this section, the stagewise procedure depicted in Fig. 2 is applied to derive optimal estimates of the repulsion–dispersion interaction parameters for a range of atoms. The parameters obtained are consistent with a distributed multipole electrostatic model derived from charge densities calculated at the M06/6-31G(d,p) level of theory.

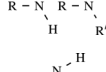## 6.1 Choice of training set and cross-validation set

The crystal structures of 106 organic molecular crystals including hydrocarbons, azahydrocarbons, oxohydrocarbons, organosulphur compounds, chlorohydrocarbons, amines, imidazoles, carboxylic acids and alcohols were collected from the CSD[47] for the purpose of the parameter estimation reported in this work. The training set was selected to contain molecules with each element in different bonding situations. For example, the training set of hydrocarbons contains alkanes and cycloalkanes with sp^3 hybridized carbons that form single bonds, aromatics with sp^2 hybridized carbons forming sigma bonds and the delocalization of electrons between the ring carbons and hydrocarbons with an alkynyl group of sp hybridized carbons that form a triple bond. Similar considerations underpinned the selection of molecules containing N, O and S, as summarized in Table 4. The molecular diagrams, CSD refcodes, numbers of molecules in the unit cell Z, space groups, R-factors and experimental temperatures are summarized in Table S1 of the ESI.†

Gas-phase molecular conformations are computed at the M06/6-31G(d,p) level of theory. The rigidity of the molecules is ascertained through $rmsd_1$ comparisons between computed and experimental conformations with *COMPACK*, giving an average $rmsd_1$ of only 0.05 Å. In a previous study by Arnautova *et al.*,[59] the C–H bond lengths of the experimental conformations were adjusted to the average experimental value from neutron diffraction data to overcome issues of unreliable hydrogen positions determined by X-ray diffraction. We found the C–H bond lengths in the gas-phase conformations to be approximately 1.087 Å, which is very close to the average experimental value of 1.089 Å derived from neutron data given in the CSD. Therefore, no modification was applied to the C–H bond lengths.

Experimentally determined enthalpies of sublimation were identified for 53 of the 106 molecules, which is significantly more than the number used in the

Table 4 Atom types and classes of compounds used for the estimation of the new potential parameters

Atom type	Bonding structures represented in dataset	Compounds classes, functional groups	Representative structures
C	Carbon bonded to four other atoms	Alkanes	$R-(CH_2)_nH$
	Carbon bonded to three other atoms	Alkenes	R1 R3 R2 R4 (C=C)
		Benzene derivatives	R—(benzene ring)
	Carbon bonded to two other atoms	Alkynes	$R-C\equiv C-R'$
H_C	Hydrogen bonded to carbon		
N	Nitrogen to three other atoms (no bonded hydrogen)	Amines	$R-N$, R'', R'
		Imines	R, R', R'' (C=N)
	Nitrogen to two other atoms (no bonded hydrogen)	Azo compounds	$R'-N=N-R'$
		Pyridine derivatives	R—(pyridine ring)
	Nitrogen with triple bond (no bonded hydrogen)	Nitriles	$R-C\equiv N$
O	Oxygen bonded to one other atom (no bonded hydrogen)	Ketones	O, R, R'
		Aldehydes	O, R, H
	Oxygen bonded to two other atoms (no bonded hydrogen)	Ethers	R–O–R'
		Esters	O, R, OR'
S	Sulphur bonded to one other atom (no bonded hydrogen)	Thiones	S, R, R'
		Thial	S, R, H
	Sulphur bonded to two other atoms (no bonded hydrogen)	Sulfides	R–S–R'
		Disulfides, polysulfides	R–S–S–R'
H_N	Hydrogen bonded to nitrogen	Amines	R–N(H)(H), R–N(H)(R')
		Imines	N–H, R, R'
H_O	Hydrogen bonded to oxygen	Alcohols	R–OH
		Carboxylic acids	R–C(=O)OH
Cl	Chlorine bonded to carbon	Chloroalkanes	R–Cl
		Chlorinated aromatics	Cl—(benzene ring)

parameterization of FIT. The sublimation enthalpies used in this work are given in Table S1 of the ESI.†

6.2 Optimized parameters

The optimal parameter estimates for the 24 atom–atom interactions occurring in the datasets are listed in Table 5, where they are also compared with the corresponding FIT parameters. The optimized parameters for sulphur interactions are further compared with two additional sets of parameters, namely those by No et al.[70] (denoted as S-No) and by Abraha et al.[71] (denoted as S-Ab). These alternative parameter sets are presented in Table 6.

The optimized parameters differ significantly from the original set. However, because of the high degree of correlation between the A_{ij} and C_{ij} parameters, large changes in their individual values do not necessarily result in a large change in the potential. Fig. 6 shows the differences in equilibrium distances and well depths of the potentials. For most pairwise interactions, these differences are relatively small. A striking exception is the O···O interaction for which we observe a significant change in the potential well depth and location of the minimum (cf. Fig. 7a), with the new parameters indicating stronger and shorter-range interactions. On the other hand, the differences between our potentials for the interactions of oxygen with other atoms and the corresponding FIT potentials are not very pronounced. This is

Table 5 Exp-6 potential parameters obtained in the FIT parameterization and in this work

Atom type		FIT[a]			This work		
i	j	A_{ij}/eV	B_{ij}/Å	C_{ij}/eV Å^6	A_{ij}/eV	B_{ij}/Å	C_{ij}/eV Å^6
C	C	3832.147	0.278	25.287	2299.288	0.278	18.020
C	H_C	689.537	0.272	5.979	449.3172	0.272	6.265
H_C	H_C	124.072	0.267	1.414	173.559	0.267	1.957
C	N	3179.515	0.271	19.007	3355.322	0.271	24.171
N	N	2638.029	0.265	14.286	3687.092	0.265	17.577
H_C	N	572.105	0.266	4.494	516.587	0.266	2.696
C	O	3022.85	0.265	17.16	1352.853	0.265	10.164
H_C	O	543.916	0.260	4.057	304.084	0.260	2.481
O	O	2384.466	0.253	11.645	963.846	0.253	18.632
C	S	3990.989	0.290	38.957	2819.374	0.290	46.499
N	S	3311.305	0.282	29.281	3760.816	0.282	31.148
H_C	S	718.118	0.284	9.211	802.131	0.284	9.891
S	S	4156.415	0.303	60.016	3401.359	0.303	95.872
C	H_N	446.952	0.242	2.374	478.038	0.242	3.561
H_C	H_N	80.422	0.238	0.561	40.211	0.238	0.842
N	H_N	370.834	0.237	1.784	297.752	0.237	0.892
H_N	H_N	52.129	0.215	0.223	78.194	0.215	0.111
H_O	C	446.952	0.242	2.374	519.271	0.242	2.488
H_O	H_C	80.422	0.238	0.561	128.676	0.238	0.224
H_O	O	352.562	0.232	1.611	231.169	0.232	0.644
H_O	H_O	52.129	0.215	0.223	61.708	0.215	0.089
C	Cl	6060.173	0.281	45.040	2627.877	0.290	39.868
H_C	Cl	1090.436	0.276	10.650	1371.320	0.276	17.708
Cl	Cl	9583.584	0.285	80.224	7940.587	0.285	67.687

[a] Parameters from (ref. 37).

Table 6 Exp-6 potential parameters for S-Ab and S-No

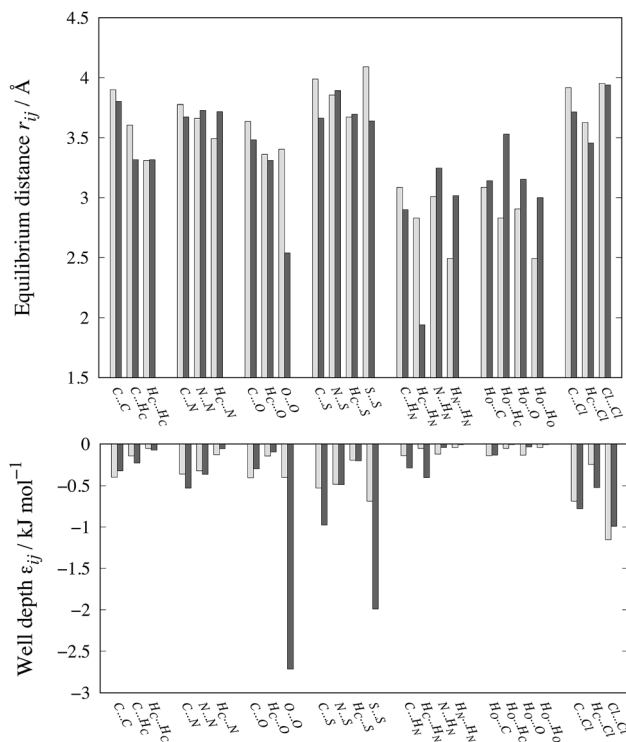| Atom type		S-Ab			S-No		
i	j	A_{ij}/eV	B_{ij}/Å	C_{ij}/eV Å^6	A_{ij}/eV	B_{ij}/Å	C_{ij}/eV Å^6
C	S	2623.650	0.308	55.295	3064.776	0.308	46.911
N	S	2176.830	0.299	41.562	2542.830	0.299	35.260
H$_C$	S	472.092	0.301	13.074	551.467	0.301	11.092
S	S	1796.306	0.345	120.918	2451.128	0.345	87.029

Fig. 6 Comparison of equilibrium distances and well depths for 24 interactions as calculated with FIT (light grey bars) and our new parameter set (dark grey bars). The data along with the results for the S-Ab and S-No parameter sets are given in Table S3 of the ESI.†

an indication of the inaccuracies that may be introduced by relying on combining rules for estimating cross-interaction parameters.

Shorter equilibrium distances and deeper wells are also observed for all S interactions apart from the H$_C$···S one (*cf.* Fig. 6 and 7b and c). We note that significant differences also exist among the FIT, S-Ab and S-No parameter sets as shown in Fig. S3 of the ESI.†

Both oxygen interactions and sulphur interactions were fitted to a number of sublimation enthalpy data. We note that no such data were used in the derivation of the FIT set. The resulting improvement in sublimation enthalpy prediction demonstrates the impact of using energetic data to fit the potentials.
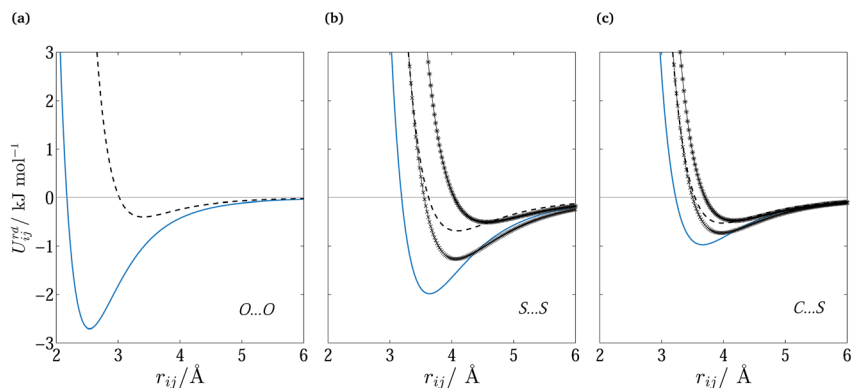
(a)   (b)   (c)

Fig. 7 Repulsion–dispersion potential curves for (a) O···O, (b) S···S and (c) C···S interactions. The optimized potential curves (continuous curves) are compared with the FIT potential curves (dashed curves) and with S-No[70] (✳) and S-Ab[71] (✗).

6.3 Performance of new parameters: sublimation enthalpy

Overall, the new parameter values result in a good fit for the experimental structures in the training set. As shown in Table 7, the sublimation enthalpy AAD is

Table 7 Comparison of accuracy of computed sublimation enthalpies and geometries with different parameter values over the training set

	Absolute sublimation enthalpy error (kJ mol^{-1})							
	FIT		This work		S-Ab		S-No	
Training set	AAD	maxAD	AAD	maxAD	AAD	maxAD	AAD	maxAD
Hydrocarbons	2.66	4.83	1.47	4.08				
Azahydrocarbons	3.43	6.80	1.28	3.56				
Oxohydrocarbons	9.46	18.22	6.88	16.66				
Organosulphur compounds	20.97	38.71	5.29	10.44	7.94	16.74	25.73	46.85
Amines, imidazoles	11.00	19.40	9.17	13.67				
Carboxylic acids, alcohols	13.98	24.93	5.94	10.50				
Chlorohydrocarbons	7.30	8.90	0.15	0.46				
Overall	8.78	38.71	4.11	16.66				

	Absolute rmsd$_{15}$ error (Å)							
	FIT		This work		S-Ab		S-No	
	Average	Max	Average	Max	Average	Max	Average	Max
Hydrocarbons	0.349	0.922	0.285	0.985				
Azahydrocarbons	0.223	0.747	0.231	0.631				
Oxohydrocarbons	0.342	0.728	0.306	0.808				
Organosulphur compounds	0.321	1.047	0.326	1.047	0.298	0.996	0.430	1.195
Amines, imidazoles	0.289	0.581	0.291	0.640				
Carboxylic acids, alcohols	0.336	0.868	0.434	0.875				
Chlorohydrocarbons	0.246	0.529	0.263	0.735				
Overall	0.305	1.047	0.309	1.047				

4.1 kJ mol^{-1}, which is 53% smaller than the corresponding FIT value while the average rmsd$_{15}$ of 0.31 Å is practically identical to that achieved by FIT. In fact, for hydrocarbons and azahydrocarbons, the achieved sublimation enthalpy AADs of less than 2 kJ mol^{-1} are similar to the errors observed with some dispersion-corrected DFT methods.[7] There is also a decrease in the spread of the sublimation enthalpy errors, with a maxAD value of 16.7 kJ mol^{-1} compared to 38.7 kJ mol^{-1} with FIT.

In addition to the training set, we employ a cross-validation set consisting of 39 crystal structures for representative molecules for all the classes of compounds considered here (see Table S2 in the ESI†). For six of these structures, the subli-mation enthalpy is also available. The criteria for the choice of the cross-validation set were similar to those for the training set (*cf.* Section 3.1) although, due to the limited availability of such data for rigid molecules, the requirements regarding experimental error were less stringent in some cases. The sublimation enthalpy results reported in Table 8 indicate similar improvements to those for the training set (*cf.* Table 7). However, the sublimation enthalpy AAD of 7.87 kJ mol^{-1} is larger than the corresponding value for the training set. This may be due to the relative sparsity of energetic data, which leads to reduced statistical significance for the parameters. We also note that some of the experi-mental sublimation enthalpy values in the cross-validation set are less reliable than the enthalpies reported for the compounds in the training set.

Fig. 8a shows parity plots between experimental and computed sublimation enthalpies for both the training and cross-validation sets. A significant improvement over the FIT set is evident across both sets. Fig. 8b focuses on the

Table 8 Comparison of accuracy of computed sublimation enthalpies and geometries for different parameter values over the cross-validation set

	Absolute sublimation enthalpy error (kJ mol^{-1})							
	FIT		This work		S-Ab		S-No	
Training set	AAD	maxAD	AAD	maxAD	AAD	maxAD	AAD	maxAD
Hydrocarbons	8.65	13.49	8.31	16.82				
Azahydrocarbons	9.51	9.51	7.49	7.49				
Amines, imidazoles	11.45	11.45	4.91	4.91				
Carboxylic acids, alcohols	23.26	23.26	9.87	9.87				
Overall	11.69	23.26	7.87	16.82				

|	Absolute rmsd$_{15}$ error (Å)							
	FIT		This work		S-Ab		S-No	
	Average	Max	Average	Max	Average	Max	Average	Max
Hydrocarbons	0.201	0.286	0.169	0.285				
Azahydrocarbons	0.402	0.747	0.317	0.433				
Oxohydrocarbons	0.147	0.188	0.197	0.289				
Organosulphur compounds	0.239	0.340	0.275	0.499	0.221	0.390	0.276	0.450
Amines, imidazoles	0.327	0.574	0.275	0.377				
Carboxylic acids, alcohols	0.526	1.828	0.579	1.537				
Chlorohydrocarbons	0.246	0.316	0.235	0.311				
Overall	0.294	1.828	0.282	1.537				
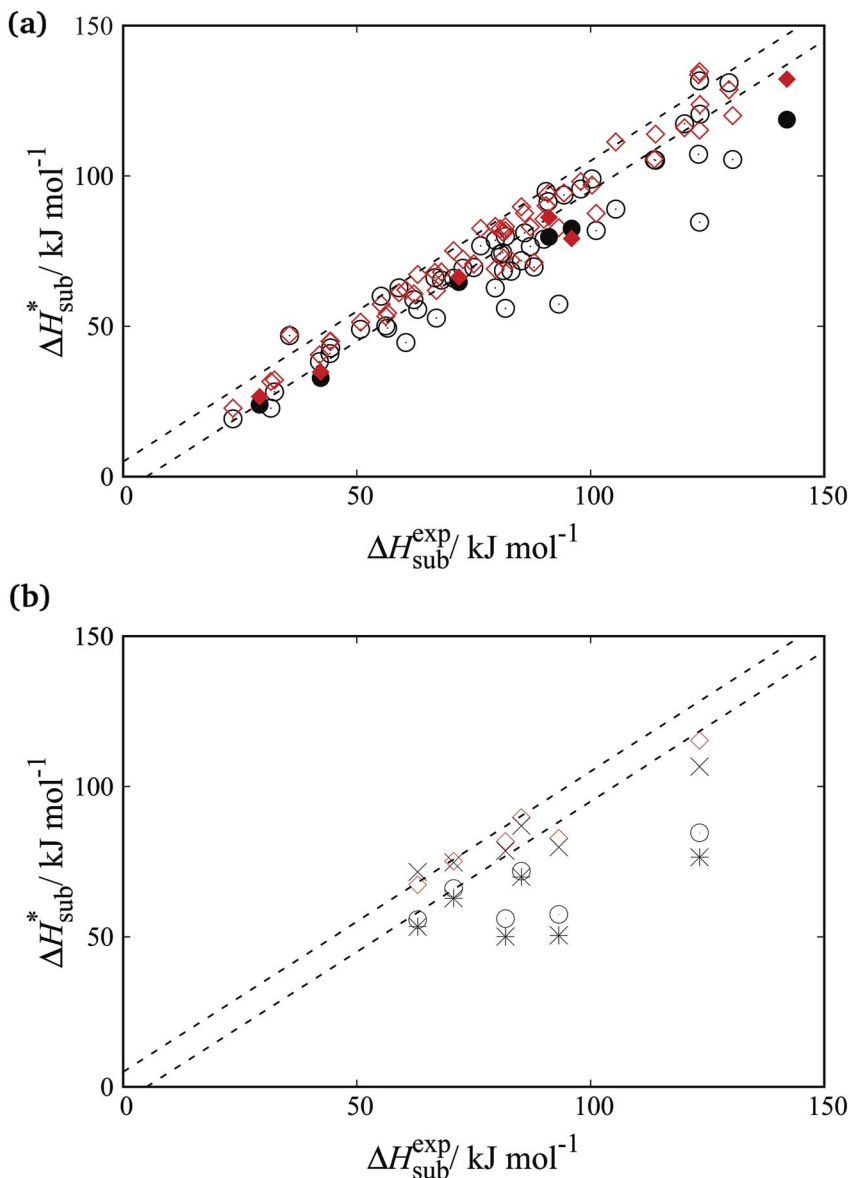
Fig. 8 Parity plots of experimental and predicted sublimation enthalpies with different parameter sets. The diagonal dashed lines (- - -) indicate experimental error bounds. (a) Training and cross-validation sets (empty and filled symbols respectively). Circles (●) and diamonds (◇) indicate values calculated with FIT parameters and the new parameters respectively. (b) Sublimation enthalpies for organosulphur compounds. FIT parameters (○), S-Ab (✕), S-No (✳) and this work (◇).

organosulphur compounds. It is clear that the accuracy of sublimation enthalpy predictions varies substantially across the previously derived parameter sets (FIT, S-No, and S-Ab). The improved predictive accuracy of the new parameters is important as the study of molecular crystals containing sulphur has so far been hampered by the limited availability of reliable transferable parameters.
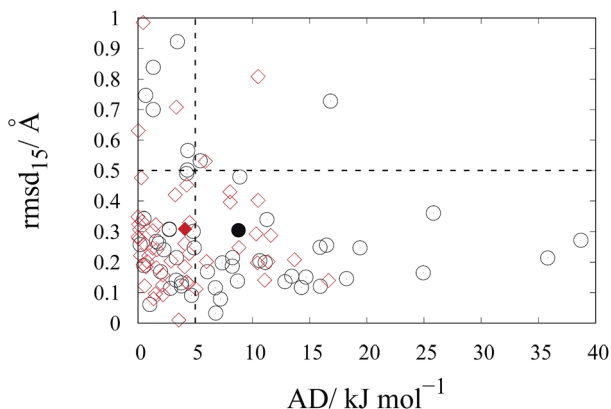
Fig. 9 Rmsd$_{15}$ relative to the corresponding absolute error in sublimation enthalpy, AD, for all the compounds in the training set calculated for FIT (○) and this work (◇). Filled symbols (● and ◆) represent the corresponding averages. The dashed lines (■ ■ ■) indicate the acceptable maximum errors in sublimation enthalpy (5 kJ mol^{-1}) and rmsd$_{15}$ (0.5 Å).

6.4   Performance of new parameters: rmsd$_{15}$

As mentioned in previous sections, the rmsd$_{15}$ between the optimized unit cells and the experimentally observed ones is also used to assess the ability of our optimal parameter estimates to accurately predict unit cell geometries. An rmsd$_{15}$ below 0.5 Å is generally considered to indicate a good degree of agreement between two structures. In our case, the average rmsd$_{15}$ over the entire training set was 0.31 Å. The rmsd$_{15}$ averages for each separate set, shown in Table 7, are below 0.5 Å. Overall, we can conclude that there is a good agreement with the experimental structures for each class although a few individual structures show rmsd$_{15}$ values nearer 1.

As indicated by the entries in the last rows of Tables 7 and 8, our new parameter set does not have a clear overall advantage over FIT in terms of rmsd$_{15}$. This is partly explained by the fact that we used a different metric for geometry in our objective function. In our methodology, improved geometry reproduction could be achieved by setting $w^G \gg w^E$), thereby placing greater importance on the geometry terms than the energy terms. However, the results presented here demonstrate that using equal weights leads to a significant increase in the accuracy of the computed sublimation enthalpies while maintaining good accuracy in geometry reproduction. In particular, as shown in Fig. 9, the new parameters lead to fewer points showing large errors in the sublimation enthalpy (>5 kJ mol^{-1}) or/and in the rmsd$_{15}$ (>0.5 Å).

7   Concluding remarks

The fundamental premise of the work reported in this paper is that the values of the repulsion–dispersion parameters estimated from experimental data depend on the model of electrostatic interactions¶ used in this estimation. Accordingly,

---

¶ And, in the case of flexible molecules, the model used for intramolecular energy contributions.

this electrostatic model needs to be the same as that used in the subsequent CSP calculations. The approach proposed here allows the systematic reparameterization of the repulsion–dispersion model to derive transferable parameters that are consistent with the rest of the lattice energy model. This is particularly important in the context of current CSP methodologies which are relying on increasingly sophisticated representations of electrostatic and intramolecular contributions based on *ab initio* quantum mechanical calculations.

The estimation of the repulsion–dispersion parameters in the lattice energy model has been formulated mathematically as a weighted least-squares minimization of the deviation between the computed and experimentally measured crystal geometries and sublimation enthalpies. Important aspects of our formulation are the weighting and scaling schemes used for balancing the contributions of different elements of the experimental dataset. The proposed solution algorithm aims to mitigate the large computational cost associated with this problem and to reduce the risk of the minimization being trapped in local minima.

The feasibility and effectiveness of the proposed approach were demonstrated by the estimation of a set of atom–atom interaction parameters for the isotropic Buckingham potential, consistent with distributed multipole electrostatics derived from charge densities computed *via* isolated-molecule quantum mechanical calculations at the M06/6-31G(d,p) level of theory.|| Interaction parameters between unlike atom types were also included directly in the estimation instead of being approximated *via* combining rules. The study reported here focused on organic molecular crystals with N, O, S and Cl atoms, and made use of a training dataset containing 106 crystal geometries and the sublimation enthalpies for 53 of these structures. A separate set of 39 structures (including 6 sublimation enthalpy values) was used for cross-validation of the derived parameter estimates. Overall, compared to the commonly used FIT parameter set, the new parameter values were found to result in significantly improved sublimation enthalpy predictions while maintaining a comparable quality of geometry reproduction.

In the work reported here, the B_{ij} parameters of the Buckingham potential were kept fixed at the corresponding FIT values. This was mainly done in order to avoid the numerical problems caused by the unphysical predictions of this potential at low interatomic separation distances. Including these parameters in the estimation set could result in improved predictive accuracy. However, with the availability of systematic ways of estimating reliable and consistent parameter values for any form of repulsion–dispersion potential, it may be worth considering alternative potential forms that do not exhibit such unphysical behavior in the first place.

Data statement

All underlying data supporting this article are available in the ESI.†

Conflicts of interest

There are no conflicts to declare.

|| Parameter values consistent with QM calculations at the HF/6-31G(d,p) and MP2/6-31G(d,p) levels of theory are reported elsewhere.[72]

Acknowledgements

Notes and references

1 A. M. Reilly, A. M. Cooper, C. S. Adjiman, S. Bhattacharya, D. Boese, J. G. Brandenburg, P. J. Bygrave, R. Bylsma, J. E. Campbell, R. Car, D. H. Case, R. Gadha, J. C. Cole, K. Cosburn, H. M. Cuppen, F. Curtis, G. M. Day, R. A. Distasio Jr, A. Dzyabchenko, B. P. van Eijck, D. M. Elking, J. A. van den Ende, J. C. Facelli, M. B. Ferraro, L. Fusti-Molnar, C. A. Gatsiou, T. S. Gee, R. de Gelder, L. M. Ghiringhelli, H. Goto, S. Grimme, R. Guo, D. W. M. Hofmann, J. Hoja, R. K. Hylton, L. Luzzolino, W. Jankiewicz, D. T. de Jong, J. Kendrick, N. J. J. de Klerk, H. Y. Ko, L. N. Kuleshova, X. Li, S. Lohani, F. J. J. Leusen, A. M. Lund, J. Lv, Y. Ma, N. Marom, A. E. Masunov, P. McCabe, D. P. McMahon, H. Meekes, M. P. Metz, A. J. Misquitta, S. Mohamed, B. Monserrat, R. J. Needs, M. A. Neumann, J. Nyman, S. Obata, H. Oberhofer, A. R. Oganov, A. M. Orendt, G. I. Pagola, C. C. Pantelides, C. J. Pickard, R. Podeszwa, L. S. Price, S. L. Price, A. Pulido, M. Read, K. Reuter, E. Schneider, C. Schober, G. P. Shields, P. Singh, I. J. Sugden, K. Szalewicz, C. R. Taylor, A. Tkatchenko, M. E. Tuckerman, F. Vacarro, M. Vasileiadis, Á. Vásquez-Mayagoittia, L. Vogt, Y. Wang, R. E. Watson, G. A. de Wijs, J. Yang, Q. Zhu and C. R. Groom, *Acta Crystallogr., Sect. B: Struct. Sci., Cryst. Eng. Mater.*, 2016, **72**, 439–459.
2 M. Vasileiadis, A. V. Kazantsev, P. G. Karamertzanis, C. S. Adjiman and C. C. Pantelides, *Acta Crystallogr., Sect. B: Struct. Sci.*, 2012, **68**, 677–685.
3 A. T. Hulme and S. L. Price, *J. Chem. Theory Comput.*, 2007, **3**, 1597–1608.
4 S. Grimme, J. Antony, S. Ehrlich and H. Krieg, *J. Chem. Phys.*, 2010, **132**, 154104.
5 M. A. Neumann and M. A. Perrin, *J. Phys. Chem. B*, 2005, **109**, 15531–15541.
6 A. Tkatchenko and M. Scheffler, *Phys. Rev. Lett.*, 2009, **102**, 073005.
7 A. Otero-De-La-Roza and E. R. Johnson, *J. Chem. Phys.*, 2012, **137**, 054103.
8 J. Moellmann and S. Grimme, *J. Phys. Chem. C*, 2014, **118**, 7615–7621.
9 H. Sun, *J. Phys. Chem. B*, 1998, **102**, 7338–7364.
10 P. Dauber-Osguthorpe, V. A. Roberts, D. J. Osguthorpe, J. Wolff, M. Genest and A. T. Hagler, *Proteins: Struct., Funct., Bioinf.*, 1988, **4**, 31–47.
11 G. M. Day, *Crystallogr. Rev.*, 2011, **17**, 3–52.
12 G. M. Day, W. D. S. Motherwell and W. Jones, *Phys. Chem. Chem. Phys.*, 2007, **9**, 1693–1704.
13 M. A. Neumann, *J. Phys. Chem. B*, 2008, **112**, 9810–9829.
14 M. Jeziorska, W. Cencek, K. Patkowski, B. Jeziorski and K. Szalewicz, *J. Chem. Phys.*, 2007, **127**, 124303.
15 S. L. Price, M. Leslie, G. W. A. Welch, M. Habgood, L. S. Price, P. G. Karamertzanis and G. M. Day, *Phys. Chem. Chem. Phys.*, 2010, **12**, 8478–8490.

16 M. Habgood, I. J. Sugden, A. V. Kazantsev, C. S. Adjiman and C. C. Pantelides, *J. Chem. Theory Comput.*, 2015, **11**, 1957–1969.

17 I. Sugden, C. S. Adjiman and C. C. Pantelides, *Acta Crystallogr., Sect. B: Struct. Sci., Cryst. Eng. Mater.*, 2016, **72**, 864–874.

18 J. P. M. Lommerse, W. D. S. Motherwell, H. L. Ammon, J. D. Dunitz, A. Gavezzotti, D. W. M. Hofmann, F. J. J. Leusen, W. T. M. Mooij, S. L. Price, B. Schweizer, M. U. Schmidt, B. P. van Eijck, P. Verwer and D. E. Williams, *Acta Crystallogr., Sect. B: Struct. Sci.*, 2000, **56**, 697–714.

19 W. D. S. Motherwell, H. L. Ammon, J. D. Dunitz, A. Dzyabchenko, P. Erk, A. Gavezzotti, D. W. M. Hofmann, F. J. J. Leusen, J. P. M. Lommerse, W. T. M. Mooij, S. L. Price, H. Scheraga, B. Schweizer, M. U. Schmidt, B. P. van Eijck, P. Verwer and D. E. Williams, *Acta Crystallogr., Sect. B: Struct. Sci.*, 2002, **58**, 647–661.

20 G. M. Day, W. D. S. Motherwell, H. L. Ammon, S. X. M. Boerrigter, R. G. Della Valle, E. Venuti, A. Dzyabchenko, J. D. Dunitz, B. Schweizer, B. P. van Eijck, P. Erk, J. C. Facelli, V. E. Bazterra, M. B. Ferraro, D. W. M. Hofmann, F. J. J. Leusen, C. Liang, C. C. Pantelides, P. G. Karamertzanis, S. L. Price, T. C. Lewis, H. Nowell, A. Torrisi, H. A. Scheraga, Y. A. Arnautova, M. U. Schmidt and P. Verwer, *Acta Crystallogr., Sect. B: Struct. Sci.*, 2005, **61**, 511–527.

21 G. M. Day, T. G. Cooper, A. J. Cruz-Cabeza, K. E. Hejczyk, H. L. Ammon, S. X. M. Boerrigter, J. S. Tan, R. G. Della Valle, E. Venuti, J. Jose, S. R. Gadre, G. R. Desiraju, T. S. Thakur, B. P. van Eijck, J. C. Facelli, V. E. Bazterra, M. B. Ferraro, D. W. M. Hofmann, M. A. Neumann, F. J. J. Leusen, J. Kendrick, S. L. Price, A. J. Misquitta, P. G. Karamertzanis, G. W. A. Welch, H. A. Scheraga, Y. A. Arnautova, M. U. Schmidt, J. van de Streek, A. K. Wolf and B. Schweizer, *Acta Crystallogr., Sect. B: Struct. Sci.*, 2009, **65**, 107–125.

22 D. A. Bardwell, C. S. Adjiman, Y. A. Arnautova, E. Bartashevich, S. X. M. Boerrigter, D. E. Braun, A. J. Cruz-Cabeza, G. M. Day, R. G. Della Valle, G. R. Desiraju, B. P. van Eijck, J. C. Facelli, M. B. Ferraro, D. Grillo, M. Habgood, D. W. M. Hofmann, F. Hofmann, K. V. J. Jose, P. G. Karamertzanis, A. V. Kazantsev, J. Kendrick, L. N. Kuleshova, F. J. J. Leusen, A. V. Maleev, A. J. Misquitta, S. Mohamed, R. J. Needs, M. A. Neumann, D. Nikylov, A. M. Orendt, R. Pal, C. C. Pantelides, C. J. Pickard, L. S. Price, S. L. Price, H. A. Scheraga, J. van de Streek, T. S. Thakur, S. Tiwari, E. Venuti and I. K. Zhitkov, *Acta Crystallogr., Sect. B: Struct. Sci.*, 2011, **67**, 535–551.

23 S. M. Woodley and R. Catlow, *Nat. Mater.*, 2008, **7**, 937–946.

24 C. C. Pantelides, C. S. Adjiman and A. V. Kazantsev, in *General Computational Algorithms for Ab Initio Crystal Structure Prediction for Organic Molecules*, ed. S. Atahan-Evrenk and A. Aspuru-Guzik, Springer International Publishing, Cham, 2014, pp. 25–58.

25 P. G. Karamertzanis and C. C. Pantelides, *J. Comput. Chem.*, 2005, **26**, 304–324.

26 P. G. Karamertzanis and C. C. Pantelides, *Mol. Phys.*, 2007, **105**, 273–291.

27 A. V. Kazantsev, P. G. Karamertzanis, C. C. Pantelides and C. S. Adjiman, in *Process Systems Engineering*, Wiley-VCH Verlag GmbH and Co. KGaA, 2014, vol. 6, pp. 1–42.

28 A. V. Kazantsev, P. G. Karamertzanis, C. S. Adjiman and C. C. Pantelides, *J. Chem. Theory Comput.*, 2011, **7**, 1998–2016.

29 A. J. Stone and M. Alderton, *Mol. Phys.*, 1985, **56**, 1047–1064.

30 A. J. Stone, *J. Chem. Theory Comput.*, 2005, **1**, 1128–1132.

31 D. E. Williams and S. R. Cox, *Acta Crystallogr., Sect. B: Struct. Sci.*, 1984, **40**, 404–417.

32 D. S. Coombes, S. L. Price, D. J. Willock and M. Leslie, *J. Phys. Chem.*, 1996, **100**, 7352–7360.

33 T. Beyer and S. L. Price, *J. Phys. Chem. B*, 2000, **104**, 2647–2655.

34 S. R. Cox, L.-Y. Hsu and D. E. Williams, *Acta Crystallogr., Sect. A: Cryst. Phys., Diffr., Theor. Gen. Crystallogr.*, 1981, **37**, 293–301.

35 D. E. Williams and D. J. Houpt, *Acta Crystallogr., Sect. B: Struct. Sci.*, 1986, **42**, 286–295.

36 L.-Y. Hsu and D. E. Williams, *Acta Crystallogr., Sect. A: Cryst. Phys., Diffr., Theor. Gen. Crystallogr.*, 1980, **36**, 277–281.

37 CPOSS Website, The FIT and WILL01 empirical "repulsion–dispersion" potentials, 2014, http://www.chem.ucl.ac.uk/cposs/dmacrys/fit_and_will01_empirical_potentials.htm, last accessed, 04 March 2018.

38 D. E. Williams, *J. Comput. Chem.*, 2001, **22**, 1154–1166.

39 Y. A. Arnautova, A. Jagielska, J. Pillardy and H. A. Scheraga, *J. Phys. Chem. B*, 2003, **107**, 7143–7154.

40 A. T. Hagler, E. Huler and S. Lifson, *J. Am. Chem. Soc.*, 1974, **96**, 5319–5327.

41 A. T. Hagler and S. Lifson, *J. Am. Chem. Soc.*, 1974, **96**, 5327–5335.

42 E. O. Pyzer-Knapp, H. P. G. Thompson and G. M. Day, *Acta Crystallogr., Sect. B: Struct. Sci., Cryst. Eng. Mater.*, 2016, **72**, 477–487.

43 A. J. Stone, *J. Chem. Theory Comput.*, 2005, **1**, 1128–1132.

44 S. Brodersen, S. Wilke, F. J. J. Leusen and G. Engel, *Phys. Chem. Chem. Phys.*, 2003, **5**, 4923–4931.

45 G. M. Day, W. D. S. Motherwell and W. Jones, *Cryst. Growth Des.*, 2005, **5**, 1023–1033.

46 W. T. M. Mooij and F. J. J. Leusen, *Phys. Chem. Chem. Phys.*, 2001, **3**, 5063–5066.

47 F. H. Allen, *Acta Crystallogr., Sect. B: Struct. Sci.*, 2002, **58**, 380–388.

48 R. G. Little, D. Pautler and P. Coppens, *Acta Crystallogr., Sect. B: Struct. Crystallogr. Cryst. Chem.*, 1971, **27**, 1493–1499.

49 P. Coppens, T. M. Sabine, G. Delaplane and J. A. Ibers, *Acta Crystallogr., Sect. B: Struct. Crystallogr. Cryst. Chem.*, 1969, **25**, 2451–2458.

50 D. E. Williams, *J. Comput. Chem.*, 2001, **22**, 1–20.

51 R. Hundt, J. C. Schön and M. Jansen, *J. Appl. Crystallogr.*, 2006, **39**, 6–16.

52 J. A. Chisholm and S. Motherwell, *J. Appl. Crystallogr.*, 2005, **38**, 228–231.

53 P. J. Linstrom and W. G. Mallard, *J. Chem. Eng. Data*, 2001, **46**, 1059–1063.

54 U. Westhaus, T. Dröge and R. Sass, *Fluid Phase Equilib.*, 1999, **158**, 429–435.

55 J. S. Chickos, *Netsu Sokutei*, 2003, **30**, 116–124.

56 L. Lorenzo Maschio, B. Civalleri, P. Ugliengo and A. Gavezzotti, *J. Phys. Chem. A*, 2011, **115**, 11179–11186.

57 A. Otero-de-la Roza and E. R. Johnson, *J. Chem. Phys.*, 2012, **137**, 054103.

58 A. M. Reilly and A. Tkatchenko, *J. Chem. Phys.*, 2013, **139**, 024705.

59 Y. A. Arnautova, J. Pillardy, C. Czaplewski and H. A. Scheraga, *J. Phys. Chem. B*, 2003, **107**, 712–723.

60 A. Gavezzotti, *Theoretical Aspects and Computer Modeling of the Molecular Solid State*, John Wiley & Sons, 1997, p. 97.

61 I. M. Sobol, *USSR Computational Mathematics and Mathematical Physics*, 1967, vol. 7, pp. 86–112.

62 P. Bratley and B. L. Fox, *ACM Trans. Math Software*, 1988, **14**, 88–100.

63 P. G. Karamertzanis, PhD thesis, Imperial College London, 2004.

64 C. G. Broyden, *IMA J. Appl. Math.*, 1970, **6**, 76–90.

65 A. J. Stone and C.-S. Tong, *J. Comput. Chem.*, 1994, **15**, 1377–1392.

66 H. H. Y. Tsui and S. L. Price, *CrystEngComm*, 1999, **1**, 24–32.

67 H. Sun, *J. Phys. Chem. B*, 1998, **102**, 7338–7364.

68 M. J. Frisch, G. W. Trucks, H. B. Schlegel, G. E. Scuseria, M. A. Robb, J. R. Cheeseman, G. Scalmani, V. Barone, B. Mennucci, G. A. Petersson, H. Nakatsuji, M. Caricato, X. Li, H. P. Hratchian, A. F. Izmaylov, J. Bloino, G. Zheng, J. L. Sonnenberg, M. Hada, M. Ehara, K. Toyota, R. Fukuda, J. Hasegawa, M. Ishida, T. Nakajima, Y. Honda, O. Kitao, H. Nakai, T. Vreven, J. A. Montgomery Jr, J. E. Peralta, F. Ogliaro, M. Bearpark, J. J. Heyd, E. Brothers, K. N. Kudin, V. N. Staroverov, R. Kobayashi, J. Normand, K. Raghavachari, A. Rendell, J. C. Burant, S. S. Iyengar, J. Tomasi, M. Cossi, N. Rega, J. M. Millam, M. Klene, J. E. Knox, J. B. Cross, V. Bakken, C. Adamo, J. Jaramillo, R. Gomperts, R. E. Stratmann, O. Yazyev, A. J. Austin, R. Cammi, C. Pomelli, J. W. Ochterski, R. L. Martin, K. Morokuma, V. G. Zakrzewski, G. A. Voth, P. Salvador, J. J. Dannenberg, S. Dapprich, A. D. Daniels, Ö. Farkas, J. B. Foresman, J. V. Ortiz, J. Cioslowski and D. J. Fox, *Gaussian 09*, Gaussian, Inc., Wallingford CT, 2009.

69 Y. Zhao and D. G. Truhlar, *Theor. Chem. Acc.*, 2008, **120**, 215–241.

70 K. T. No, O. Y. Kwon, S. Y. Kim, K. H. Cho, C. N. Yoon, Y. K. Kang, K. D. Gibson, M. S. Jhon and H. A. Scheraga, *J. Phys. Chem.*, 1995, **99**, 13019–13027.

71 A. Abraha and D. E. Williams, *Inorg. Chem.*, 1999, **38**, 4224–4228.

72 C.-A. Gatsiou, PhD thesis, Imperial College London, 2016.